ELSEVIER

International Journal of Solids and Structures 41 (2004) 399–411

INTERNATIONAL JOURNAL OF SOLIDS and STRUCTURES

www.elsevier.com/locate/ijsolstr

Modelling cracks in arbitrarily shaped finite bodies by distribution of dislocation

Jian-Jun Han, Manicka Dhanasekar *

Centre for Railway Engineering, Central Queensland University, Building 70, Rockhampton, Qld 4702, Australia

Received 22 March 2003; received in revised form 22 September 2003

Abstract

This paper presents an analytical method based on the principle of continuous distribution of dislocation to model curved cracks in solids of arbitrarily shaped finite geometries. Both the boundary of the finite body and the curved crack are modelled by distributed dislocation. In this method the influence function of the dislocation along the finite body boundary is reduced to a product of the Hilbert kernel with a normal function. Similarly the influence function for the curved cracks is reduced to the product of Cauchy kernel and a normal function. This approach results in a system of singular integral equations. Using the order decreasing method, the system is reduced to normal integral equations, which are solved numerically. Stress intensity factors are evaluated for a well-known crack problem and two railhead crack problems with a view to assessing the capability of the developed method to solve complex engineering problems.

Keywords: Distributed dislocation; Curved cracks; Finite solids; Stress intensity factors; Mode I fracture; Mode II fracture

1. Introduction

Almost all engineering components crack under service load sometime during their effective life. Interface cracking including debonding in surface layers, or matrix and fibres in composites, cracks emanating from rivet hole edges and railhead fracture are some examples. The cracked components under different loading regimes respond differently and contribute to the growth of the cracks. Many crack problems with simple geometries under a uniform state of stress field are presented in textbooks and monographs (for example, Sih, 1962; Murakami et al., 1987, 1992). When complex finite geometries are encountered, finite element (FE) modelling is nowadays often used, although the FE method requires significant effort in defining mesh around the crack tip and remeshing where crack growth is modelled. With a view to saving effort in remeshing for the problems containing moving discontinuities, various meshless methods (Moes et al., 1999) are reported in the literature. Unfortunately it is difficult to impose essential boundary conditions in the meshless methods. With a view to overcoming such difficulties, several researchers have

* Corresponding author. Tel.: +61-7-4930-9688/9677; fax: +61-7-4930-6984.
E-mail address: m.dhanasekar@cqu.edu.au (M. Dhanasekar).

0020-7683/$ - see front matter © 2003 Elsevier Ltd. All rights reserved.
doi:10.1016/j.ijsolstr.2003.09.045

coupled the FE with meshless methods—one of the recent papers in this topic uses a collocation approach for the coupling (Xiao and Dhanasekar, 2002). All these evidences show that the numerical methods, although well developed, still require significant research, particularly for fracture modelling. This paper describes an analytical formulation based on distributed dislocation theory for such problems, in particular where the cracks and the geometries are arbitrarily curved.

Since the pioneering work of Bilby et al. (1963, 1968) using continuous distribution of dislocation to model cracks, the distributed dislocation method has been employed to analyse various crack problems. For example, Erdogan and Gupta (1971) modelled an interface flaw in layered composites; Comninou and Schmeuser (1979) and Comninou and Chang (1985) examined the interface cracks under tension–compression or shear load with particular attention to partial closure and friction effects on radially emanating cracks from circular holes; Freund and Kim (1991) modelled spiral cracks around a strained cylindrical inclusion; Hills and Comninou (1985) and Nowell and Hills (1987) simulated edge cracks and open cracks in an elastic half-plane; Erdogan et al. (1974), Zhao and Chen (1997) and Han and Chen (2000) investigated the interaction between cracks and circular inclusions, subinterface cracks, and microvoids. The applications of this elegant method, however, were mainly focused on the physical aspects of crack problems and geometries that are restricted to infinite mediums. Furthermore, only simple configurations of the cracks such as straight lines, circles and combination of straight lines and circles are reported.

Very little research on modelling finite bodies by continuous distribution of dislocation is reported. Sheng (1987) has presented a formulation of boundary element method by dislocation distribution. Dai (2002) has reported a generalised method of modelling cracks in finite bodies by distributed dislocation and dislocation dipoles. However, this method is also restricted to simple configurations of finite bodies (for example, straight lines, circles or combinations of straight lines and circles). Subsequently, for arbitrary shaped finite bodies the boundary is required to be divided into a number of boundary elements.

To model curved cracks in finite bodies of arbitrary shapes, the method of continuous distribution of dislocation is extended in this paper. The influence function of the dislocation along the finite body boundary is reduced to a product of the Hilbert kernel and a normal function, and the influence function along the crack is reduced to the product of a Cauchy kernel and a normal function. The interaction problem between the boundary and the crack provides a system of singular integral equations. The system of singular integral equations is transformed into normal equations using the order decreasing method. The system of normal integral equations is then solved numerically using the standard methods available in the literature. The solutions provide the dislocation distribution functions along the boundary and the crack faces.

The solution of the dislocation distribution functions and the stress fields induced from the dislocation are presented first. A set of singular integral equations is then derived followed by a numerical integral method transforming the singular integral equations into normal integral equations. Three examples are presented to illustrate the validity of the method, namely a well-known standard crack problem and two complex railhead crack problems.

2. Formulation

The stress (σ_{xx}, σ_{yy}, τ_{xy}) and displacement (u_x, u_y) in two dimensional (2D) elastic bodies are defined in terms of the complex stress functions $\phi(z)$ and $\psi(z)$ provided by Muskhelishvili (1963) as shown in (1) and (2), respectively

$$\begin{aligned} \sigma_{xx} + \sigma_{yy} &= 2\lfloor \Phi(z) + \overline{\Phi(z)} \rfloor \\ \sigma_{yy} - \sigma_{xx} + 2\mathrm{i}\tau_{xy} &= 2[\bar{z}\Phi'(z) + \Psi(z)] \end{aligned} \tag{1}$$

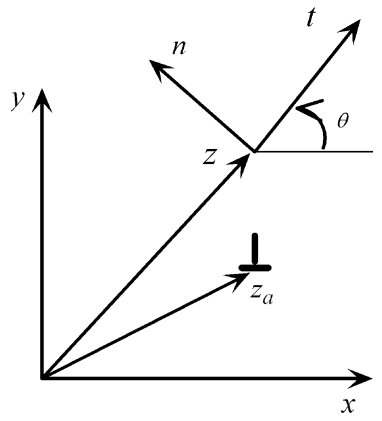

Fig. 1. A dislocation in an infinite plane.

$$2G(u_x + \mathrm{i}u_y) = \kappa\phi(z) - z\overline{\Phi(z)} - \psi(z) \tag{2}$$

where the over bar sign represents the conjugate of the complex function; and $\Phi(z) = \phi'(z)$, $\Psi(z) = \psi'(z)$, and $\kappa = (3 - v)/(1 + v)$ for plane stress, $\kappa = 3 - 4v$ for plane strain, in which v and G are Poisson's ratio and shear modulus of the material, respectively.

Bilby and Eshelby (1968) provided a solution for an edge dislocation at point z_a in an infinite plane as shown in Fig. 1 as

$$\begin{aligned} \Phi(z) &= A/(z - z_a) \\ \Psi(z) &= \overline{A}/(z - z_a) + A\overline{z_a}/(z - z_a)^2 \end{aligned} \tag{3}$$

where

$$A = G(\beta_x + \mathrm{i}\beta_y)/[\mathrm{i}\pi(1 + \kappa)] \tag{4}$$

in which β_x and β_y are the Burgers vector defined as increased displacement around the point z_a.

The normal and the tangential stress components at a point z induced from the dislocation at z_a are derived by substituting (3) into (1) and employing (t, n) coordinates with incline angle θ

$$\sigma_{nn} - \mathrm{i}\tau_{nt} = \beta_x f_x(z, z_a) + \beta_y f_y(z, z_a) \tag{5}$$

where

$$\begin{aligned} f_x(z, z_a) &= \frac{G}{\pi\mathrm{i}(1 + \kappa)}\left(\frac{1}{z - z_a} - \frac{1}{\bar{z} - \overline{z_a}} + \mathrm{e}^{2\mathrm{i}\theta}\left[\frac{1}{z - z_a} + \frac{(\bar{z} - \overline{z_a})}{(z - z_a)^2}\right]\right) \\ f_y(z, z_a) &= \frac{G}{\pi(1 + \kappa)}\left(\frac{1}{z - z_a} + \frac{1}{\bar{z} - \overline{z_a}} - \mathrm{e}^{2\mathrm{i}\theta}\left[\frac{1}{z - z_a} - \frac{(\bar{z} - \overline{z_a})}{(z - z_a)^2}\right]\right) \end{aligned} \tag{6}$$

2.1. Decomposition of original problem

Consider a finite body of arbitrary shape that is a cut-off from an infinite plane by a closed crack, as demonstrated in Fig. 2. The original problem of a curved crack in a finite body may be regarded as the superposition of two subproblems.

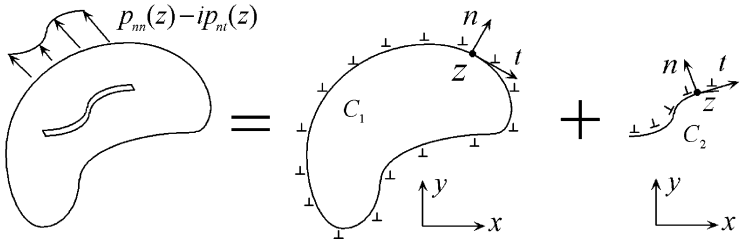

Fig. 2. Decomposition of original problem.

The first subproblem is an infinite plane with a closed curved crack and the second subproblem is an infinite plane with an open crack of arbitrary shape. Both the closed crack and the open crack are modelled by continuous distribution of dislocation.

As shown in Fig. 2, the closed crack is denoted by C_1 and the open crack by C_2. The distribution functions of Burgers vector β_x and β_y are denoted by $g_{1x}(z_a)$ and $g_{1y}(z_a)$ along C_1 and by $g_{2x}(z_a)$ and $g_{2y}(z_a)$ along C_2. The normal and tangential stress components at a point z on C_1 or C_2 induced by the distributed dislocation are obtained from the integral of the stress induced by the dislocation at point z_a as shown in (7).

$$\sigma_{nnj}(z) - \mathrm{i}\tau_{ntj}(z) = \int_{C_j} [g_{jx}(z_a) f_x(z, z_a) + g_{jy}(z_a) f_y(z, z_a)]\,\mathrm{d}z_a \tag{7}$$

where $j = 1$ for C_1 and 2 for C_2. As shown in Fig. 2, the coordinate system (t, n) at point z moves and rotates as point z moves along C_1 or C_2, and θ in (6) is a function of z.

Superposition of the two subproblems provides the solution to the original problem. From the boundary conditions along the cracks defining the finite body, the integral equation shown in (8) is derived.

$$\begin{aligned} &\int_{C_1} g_{1x}(z_a) f_x(z, z_a) + g_{1y}(z_a) f_y(z, z_a)\,\mathrm{d}z_a + \int_{C_2} g_{2x}(z_a) f_x(z, z_a) + g_{2y}(z_a) f_y(z, z_a)\,\mathrm{d}z_a \\ &\quad = p_{nn}(z) - \mathrm{i}p_{nt}(z) \quad z \text{ on } C_1 \text{ or } C_2 \end{aligned} \tag{8}$$

where $p_{nn}(z) - \mathrm{i}p_{nt}(z)$ are external normal and tangential boundary tractions prescribed to crack faces and the finite boundary.

The displacements are single-valued around the contours C_1 and C_2. These conditions lead to a set of integral equations in (9) and (10) for C_1 and C_2, respectively.

$$\int_{C_1} g_{1x}(z_a)\,\mathrm{d}z_a = 0, \quad \int_{C_1} g_{1y}(z_a)\,\mathrm{d}z_a = 0 \tag{9}$$

$$\int_{C_2} g_{2x}(z_a)\,\mathrm{d}z_a = 0, \quad \int_{C_2} g_{2y}(z_a)\,\mathrm{d}z_a = 0 \tag{10}$$

2.2. Singular integral equations

The set of integral equations shown in (8)–(10) provides the basis for solving the original problem. The right side of these equations and the kernel functions ($f_x(z, z_a)$ and $f_y(z, z_a)$) in the left side of these equations are known functions, while the dislocation distribution functions, $g_{1x}(z_a)$, $g_{1y}(z_a)$, $g_{2x}(z_a)$, $g_{2y}(z_a)$, are unknown functions.

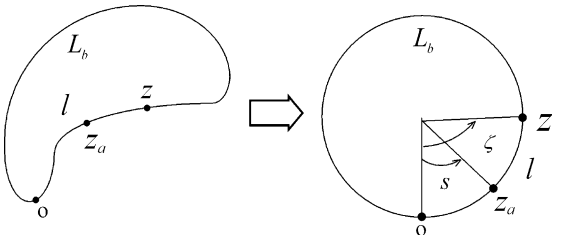

Fig. 3. Representation of an arbitrary shape as an equivalent circle.

From (6), it can be seen that (8) is a singular integral equation. It has been reported that the kernel in (8) is the Cauchy kernel when the integral contour is a straight line (Zhao and Chen, 1997), and the Hilbert kernel when the contour is a circle (Han and Chen, 2000). For arbitrary shaped integral contours, no solution is yet provided in the literature. The kernel functions vary directly depending on the shape of the boundary and that of the crack. However, as the order of these kernel functions does not change, we can reduce them to products of the Cauchy or Hilbert kernels with normal functions.

In order to expand the kernel functions into the products of singular and normal functions, as shown in Fig. 3, we express contour C_1 by $z_1(\zeta)$ in terms of an auxiliary variable ζ.

The auxiliary variable denotes the hoop angle of a circle with the same hoop length, L_b, as C_1 and has a relation with the length l between a point z and a reference point o on C_1 as

$$\zeta = 2\pi l/L_b \tag{11}$$

Substituting (11) into (6) and noting z and z_a corresponding to hoop angles ζ and s (see Fig. 3), respectively, (6) is redefined as

$$\begin{aligned} f_x(z,z_a) &= F_{1x}(\zeta,s)/2\tan((s-\zeta)/2) \\ f_y(z,z_a) &= F_{1y}(\zeta,s)/2\tan((s-\zeta)/2) \end{aligned} \tag{12}$$

where $F_{1x}(\zeta,s)$ and $F_{1y}(\zeta,s)$ are normal functions whose values are determined by

$$\begin{aligned} F_{1x}(\zeta,s) &= 2f_x(z_1(\zeta),z_1(s))\tan((s-\zeta)/2) \\ F_{1y}(\zeta,s) &= 2f_y(z_1(\zeta),z_1(s))\tan((s-\zeta)/2) \end{aligned} \tag{13}$$

When $s=\zeta$, they are defined from (6) and (13) as the limit when $s \to \zeta$

$$\begin{aligned} F_{1x}(\zeta,\zeta) &= \frac{G}{\pi \mathrm{i}(1+\kappa)z_1'(\zeta)}\left(\frac{z_1'(\zeta)}{\overline{z_1'(\zeta)}} - 1 - \mathrm{e}^{2\mathrm{i}\theta}\left[\frac{\overline{z_1'(\zeta)}}{z_1'(\zeta)}+1\right]\right) \\ F_{1y}(\zeta,\zeta) &= \frac{-G}{\pi(1+\kappa)z_1'(\zeta)}\left(\frac{z_1'(\zeta)}{\overline{z_1'(\zeta)}} + 1 + \mathrm{e}^{2\mathrm{i}\theta}\left[\frac{\overline{z_1'(\zeta)}}{z_1'(\zeta)}-1\right]\right) \end{aligned} \tag{14}$$

Similarly we express the contour C_2 as $z_2(s)$ function of a length from a point to midpoint of C_2 and by expanding the kernel functions into products of the Cauchy kernel with normal functions.

$$\begin{aligned} f_x(z,z_a) &= F_{2x}(\zeta,s)/(s-\zeta) \\ f_y(z,z_a) &= F_{2y}(\zeta,s)/(s-\zeta) \end{aligned} \tag{15}$$

Normal functions $F_{2x}(\zeta,s)$ and $F_{2y}(\zeta,s)$ are given by

$$\begin{aligned} F_{2x}(\zeta,s) &= (s-\zeta)f_x(z_2(\zeta),z_2(s)) \\ F_{2y}(\zeta,s) &= (s-\zeta)f_y(z_2(\zeta),z_2(s)) \end{aligned} \tag{16}$$

When $s = \zeta$, they are defined from (6) and (16) as the limit when $s \to \zeta$

$$\begin{aligned} F_{2x}(\zeta,\zeta) &= \frac{G}{\pi \mathrm{i}(1+\kappa)z_2'(\zeta)}\left(\frac{z_2'(\zeta)}{\overline{z_2'(\zeta)}} - 1 - \mathrm{e}^{2\mathrm{i}\theta}\left[\frac{\overline{z_2'(\zeta)}}{z_2'(\zeta)} + 1\right]\right) \\ F_{2y}(\zeta,\zeta) &= \frac{-G}{\pi(1+\kappa)z_2'(\zeta)}\left(\frac{z_2'(\zeta)}{\overline{z_2'(\zeta)}} + 1 + \mathrm{e}^{2\mathrm{i}\theta}\left[\frac{\overline{z_2'(\zeta)}}{z_2'(\zeta)} - 1\right]\right) \end{aligned} \tag{17}$$

The dislocation distribution functions $g_{1x}(s)$ and $g_{1y}(s)$ are normal functions for contour C_1 with some exceptional cases of edge cracks or notches that will be presented in a separate paper. The functions $g_{2x}(s)$ and $g_{2y}(s)$, however, are singular at crack tips. Thus they are redefined as

$$\begin{aligned} g_{2x}(s) &= h_x(s)/\sqrt{L_c^2 - s^2} \\ g_{2y}(s) &= h_y(s)/\sqrt{L_c^2 - s^2} \end{aligned} \quad -L_c \leqslant s \leqslant L_c \tag{18}$$

where $h_x(s)$ and $h_y(s)$ are two normal functions; L_c denotes the half length of the crack.

Substituting (12), (15) and (18) into (8), a singular integral equation with Cauchy and Hilbert kernels is derived

$$\begin{aligned} &\int_{C_1} \frac{g_{1x}(s)F_{1x}(\zeta,s) + g_{1y}(s)F_{1y}(\zeta,s)}{2\tan((s-\zeta)/2)}\,\mathrm{d}s + \int_{C_2} \frac{h_x(s)F_{2x}(\zeta,s) + h_y(s)F_{2y}(\zeta,s)}{\sqrt{L_c^2 - s^2}(s-\zeta)}\,\mathrm{d}s \\ &\quad = p_{nn}(\zeta) - \mathrm{i}p_{nt}(\zeta) \quad \zeta \text{ on } C_1 \text{ or } C_2 \end{aligned} \tag{19}$$

By using the properties of the two kernels

$$\int_{C_1} \frac{1}{\tan((s-\zeta)/2)}\,\mathrm{d}s = 0 \tag{20}$$

$$\int_{C_2} \frac{1}{\sqrt{L_c^2 - s^2}(s-\zeta)}\,\mathrm{d}s = 0 \tag{21}$$

the singular integral equation (19) is reduced to a normal equation shown in (22)

$$\begin{aligned} &\int_{C_1} \frac{g_{1x}(s)F_{1x}(\zeta,s) - g_{1x}(\zeta)F_{1x}(\zeta,\zeta) + g_{1y}(s)F_{1y}(\zeta,s) - g_{1y}(\zeta)F_{1y}(\zeta,\zeta)}{2\tan((s-\zeta)/2)}\,\mathrm{d}s \\ &\quad + \int_{C_2} \frac{h_x(s)F_{2x}(\zeta,s) - h_x(\zeta)F_{2x}(\zeta,\zeta) + h_y(s)F_{2y}(\zeta,s) - h_y(\zeta)F_{2y}(\zeta,\zeta)}{\sqrt{L_c^2 - s^2}(s-\zeta)}\,\mathrm{d}s \\ &= p_{nn}(\zeta) - \mathrm{i}p_{nt}(\zeta) \quad \zeta \text{ on } C_1 \text{ or } C_2 \end{aligned} \tag{22}$$

To determine the unknown functions in (22), $g_{1x}(s)$, $g_{1y}(s)$, $h_x(s)$ and $h_y(s)$, they are expanded into the first kind of the Chebyshev series as shown in (23)

$$
\begin{aligned}
g_{1x}(s) &= \sum_{j=0}^{M} A_{1xj} T_j(s/\pi) \\
g_{1y}(s) &= \sum_{j=0}^{M} A_{1yj} T_j(s/\pi) \\
h_x(s) &= \sum_{j=0}^{M} A_{2xj} T_j(s/L_c) \\
h_y(s) &= \sum_{j=0}^{M} A_{2yj} T_j(s/L_c)
\end{aligned}
\tag{23}
$$

where $T_j(s)$ is the jth order Chebyshev polynomial. Substituting (23) and (18) into (9) and (10), the following relations are derived

$$
\begin{aligned}
&\sum_{j=0}^{M/2} A_{1x(2j)} \Big/ (1-4j^2) = 0 \\
&\sum_{j=0}^{M/2} A_{1y(2j)} \Big/ (1-4j^2) = 0 \\
&A_{2x0} = 0 \\
&A_{2y0} = 0
\end{aligned}
\tag{24}
$$

Considering the conditions $g_{1x}(\pi) = g_{1x}(-\pi)$ and $g_{1y}(\pi) = g_{1y}(-\pi)$, two other relations are derived as

$$
\begin{aligned}
&\sum_{j=1}^{M/2} A_{1x(2j-1)} = 0 \\
&\sum_{j=1}^{M/2} A_{1y(2j-1)} = 0
\end{aligned}
\tag{25}
$$

Substituting (25) and (24) into (23), the four functions in (23) are redefined as

$$
\begin{aligned}
g_{1x}(s) &= \sum_{j=2}^{M+1} A_{1xj} T_j^*(s/\pi) \\
g_{1y}(s) &= \sum_{j=2}^{M+1} A_{1yj} T_j^*(s/\pi) \\
h_x(s) &= \sum_{j=1}^{M} A_{2xj} T_j(s/L_c) \\
h_y(s) &= \sum_{j=1}^{M} A_{2yj} T_j(s/L_c)
\end{aligned}
\tag{26}
$$

where

$$
T_j^*(s) = \begin{cases} T_j(s) - 1/(1-j^2) & \text{when } j \text{ is even} \\ T_j(s) - s & \text{when } j \text{ is odd} \end{cases}
\tag{27}
$$

Substituting (26) and (27) into (22), and employing the Chebyshev numerical integration method, a system of linear equations is derived from (22)

$$\begin{aligned}
&\sum_{j=2}^{M+1}\sum_{k=1}^{N}\frac{A_{1xj}T_j^*(s_k/\pi)F_{1x}(\zeta_l,s_k)-A_{1xj}T_j^*(\zeta_l/\pi)F_{1x}(\zeta_l,\zeta_l)}{2\tan((s_k-\zeta_l)/2)}\delta_k\\
&\quad+\sum_{j=2}^{M+1}\sum_{k=1}^{N}\frac{A_{1yj}T_j^*(s_k/\pi)F_{1y}(\zeta_l,s_k)-A_{1xj}T_j^*(\zeta_l/\pi)F_{1y}(\zeta_l,\zeta_l)}{2\tan((s_k-\zeta_l)/2)}\delta_k\\
&\quad+\sum_{j=2}^{M+1}\sum_{k=1}^{N}\frac{A_{2xj}T_j(s_k/L_c)F_{2x}(\zeta_l,s_k)-A_{2xj}T_j(\zeta_l/L_c)F_{2x}(\zeta_l,\zeta_l)}{(s_k-\zeta_l)}\\
&\quad+\sum_{j=2}^{M+1}\sum_{k=1}^{N}\frac{A_{2yj}T_j(s_k/L_c)F_{2y}(\zeta_l,s_k)-A_{2yj}T_j(\zeta_l/L_c)F_{2y}(\zeta_l,\zeta_l)}{(s_k-\zeta_l)}=p_{nn}(\zeta_l)-\mathrm{i}p_{nt}(\zeta_l)
\end{aligned}\tag{28}$$

where

$$\begin{aligned}
s_k&=\cos((2k-1)\pi/2N)\pi \quad \text{on } C_1\\
s_k&=\cos((2k-1)\pi/2N)L_c \quad \text{on } C_2\\
\zeta_l&=\cos((2l-1)\pi/2N)\pi \quad \text{on } C_1\\
\zeta_l&=\cos((2l-1)\pi/2N)L_c \quad \text{on } C_2\\
\delta_k&=\sin((2k-1)\pi/2N)
\end{aligned}\tag{29}$$

in which the unknown coefficients A_{1xj}, A_{1yj}, A_{2xj} and A_{2yj} can be evaluated numerically.

Once these equations are solved, the stress intensity factors at the two tips of the crack are calculated from the values of the normal functions, $h_x(s)$ and $h_y(s)$, at the two tips as

$$K=K_{\mathrm{I}}+\mathrm{i}K_{\mathrm{II}}=\frac{G\mathrm{i}\pi}{(1+\kappa)\sqrt{\pi L_2}}\{h_x(L_c)+\mathrm{i}h_y(L_c)\}=\frac{G\mathrm{i}\pi}{(1+\kappa)\sqrt{\pi L_2}}\sum_{j=1}^{M}(A_{2xj}+\mathrm{i}A_{2yj})\tag{30}$$

for the tip $s=L_c$, and

$$K=K_{\mathrm{I}}+\mathrm{i}K_{\mathrm{II}}=\frac{G\mathrm{i}\pi}{(1+\kappa)\sqrt{\pi L_2}}\{h_x(-L_c)+\mathrm{i}h_y(-L_c)\}=\frac{G\mathrm{i}\pi}{(1+\kappa)\sqrt{\pi L_2}}\sum_{j=1}^{M}(-1)^j(A_{2xj}+\mathrm{i}A_{2yj})\tag{31}$$

for the tip $s=-L_c$.

A MATLAB program was developed to solve the problem of curved cracks in arbitrary shaped finite bodies subjected to loading and boundary conditions. In particular the parameters in (28) were set as $M=60$, $N=80$, and $v=0.3$. The input to the program includes the configurations of the problem and loading conditions, and the output of the program provides stress intensity factors at the crack tips.

3. Numerical examples

To assess the performance of the developed continuous distribution dislocation method, three examples were considered. The first is a well-known crack problem (Murakami et al., 1987) and the second is a railhead problem containing a straight crack inclined at various angles to the vertical symmetry axis of the rail. The third problem is a railhead containing a curved crack.

3.1. Example #1

A rectangular plate (height $2h$, width $2w$) that contains a straight central crack of length $2a$, is subjected to a uniform tensile stress perpendicular to the direction of the crack. The problem was solved for varying lengths of cracks (Semi-crack length varying from zero to $0.7w$). Two sizes of plates, one square $h/w = 1$ and one rectangular, $h/w = 0.5$, were also considered.

The variation of the stress intensity factor normalized by $K_0 = \sigma\sqrt{\pi a}$ is shown in Fig. 4. The solutions provided by Dai (2002) and those predicted by the current method are also shown in Fig. 4. It can be seen that the normalized SIF tends towards unity as the crack length decreases to zero. This shows that the plate can be regarded as an infinite plane for small cracks. As the crack size increases, the normalized SIF increases and is far bigger than unity for larger cracks (in some case as high as 3).

It could be seen that the results of the current method agree very well with the results of Dai (2002) as shown in Fig. 4. This agreement validates the method for simple standard cases. To illustrate the applicability of the method to a somewhat more complex problem, a cracked railhead section was considered as Example #2.

3.2. Example #2

A standard rail section UIC 71 (Profillids, 1995) was used for this purpose (Fig. 5). The overall height of the section is 186 mm, the width of the head is 76 mm and the base is 160 mm. Since the rail web is relatively long and thin, the boundary condition at the base was considered to be less significant to the railhead stresses. Consequently the bottom surface of the rail foot is subjected to uniform force to balance a distributed uniform load P applied to the railhead symmetrically as shown in Fig. 5. Width of the load P, w, is 10 mm. The Poisson's ratio and the Young's modulus of the rail steel are assumed as 0.3 and 210 GPa, respectively.

In this problem, a 5 mm crack is positioned at 165 mm above the rail foot within the railhead. The line of crack was assumed to make an angle φ with the vertical axis. When the angle $\varphi = 0°$, the cracked rail is said to possess vertical split head (VSH) defect. The stress intensity factor (SIF) for mode I, K_I, has a maximum value for this VSH defect, while the mode II SIF, K_{II}, is zero.

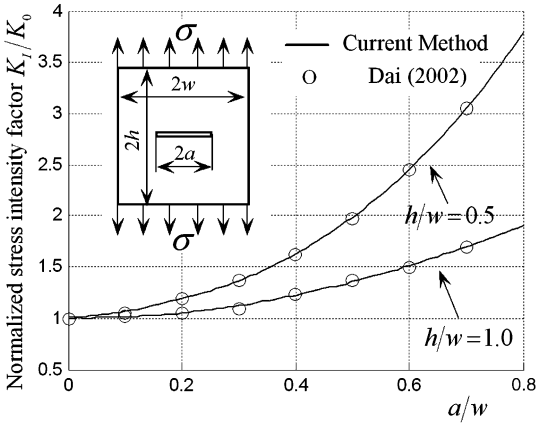

Fig. 4. Effect of crack size on mode I stress intensity factor.

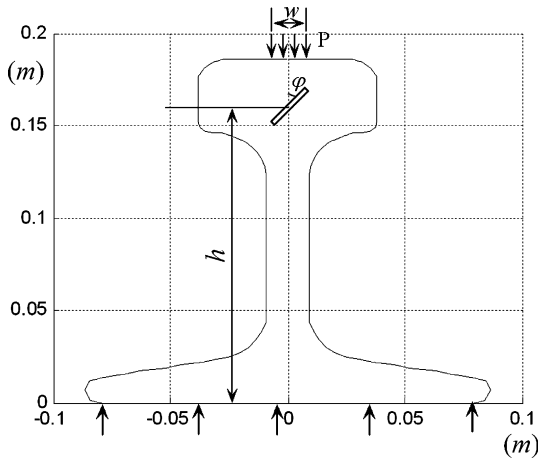

Fig. 5. Profile of UIC71 rail section.

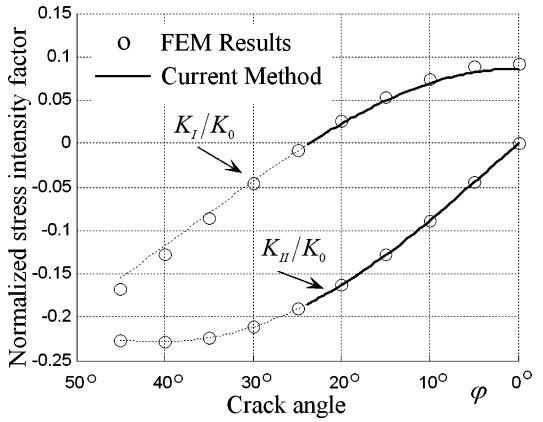

Fig. 6. Effect of crack angle on stress intensity factors.

Analyses for the range of angles φ from 0° to 45° were considered. The stress intensity factors, K_{I} and K_{II}, were normalized using a factor $K_0 = P\sqrt{\pi a}$. The normalized SIF are plotted against the crack angle φ in Fig. 6.

With a view to validating these results, FE analyses of the rail section containing the crack were carried out. ABAQUS was used for this purpose. A typical mesh used for the analysis is shown in Fig. 7. Eight noded plane strain elements (CPE8) were used. These elements were collapsed as quarter-point singular elements around the crack tips. The mesh typically contained 1075 elements and 3347 nodes. SIFs were extracted from interaction integrals (Shih and Asaro, 1988).

Fig. 6 also shows the results obtained from the FE analysis. It can be seen that the results obtained from the method presented in this paper agree very well with those of the FE analysis, thus validating the new method. From Fig. 6 it could be concluded that mode I SIF, K_{I}, attains a maximum value for VSH defect and reduces steadily with the increase in the angle. When $\varphi \geqslant 24°$, K_{I} becomes negative, implying that the crack will close. The mode II SIF on the other hand increases with the increase in φ angle. The results in

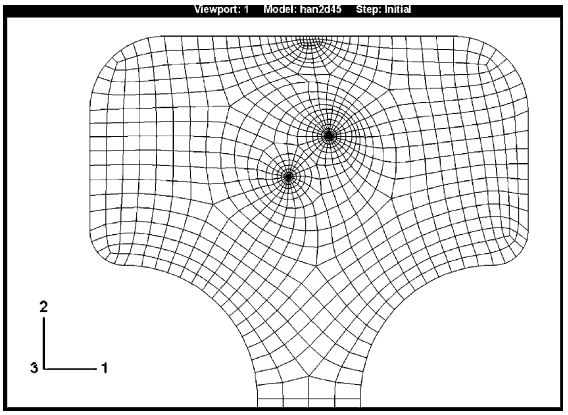

Fig. 7. FE mesh of a railhead containing a straight crack.

which the mode I SIF provides negative values, as shown by the dashed lines in Fig. 6, lead to inappropriate solutions. This is because that the crack faces near the tips for these cases are no longer traction-free due to re-establishment of contact. The complex cases require further development of this method.

3.3. Example #3

For the railhead and loading shown in Example #2, a curved crack of length 3 mm was considered in the third example as shown in Fig. 8. The crack has three segments—the central part being a straight line inclined to the vertical axis at an angle of 45° connected to the two segments are curves anti-symmetric to the horizontal axis as shown in Fig. 8. The two tips of the curved crack point to the vertical direction. This example is used to calculate the SIF by the current distributed dislocation method and the FE method (using ABAQUS). The finite element mesh used in the analysis is shown in Fig. 9.

The normalized SIF for modes I and II fracture obtained for the problem of railhead containing a curved crack are listed in Table 1. It can be seen that the results obtained from the method presented in this paper agree very well with those from the FE simulation, thus validating the distributed dislocations method for arbitrary shaped cracks.

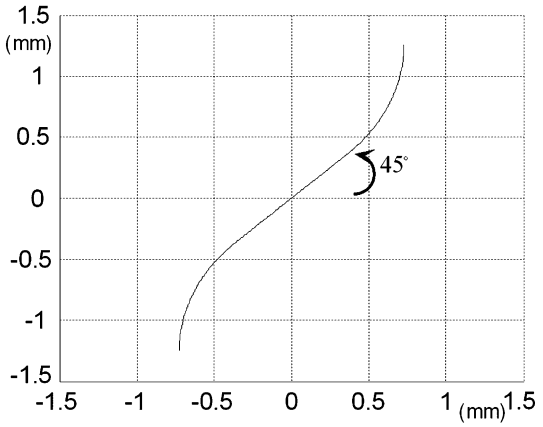

Fig. 8. Configuration of the curved crack.

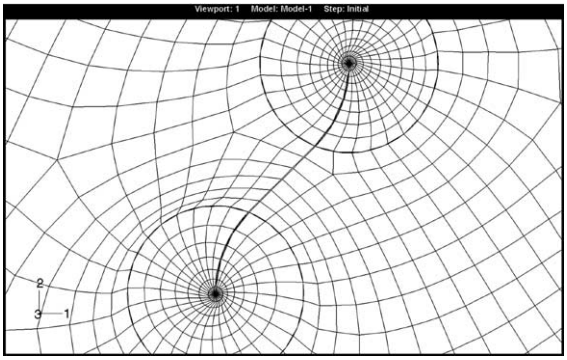

Fig. 9. FE mesh around the curved crack.

Table 1
Normalized SIFs for the railhead containing a curved crack

	Mode I SIF K_I/K_0		Mode II SIF K_{II}/K_0	
	Up tip	Low tip	Up tip	Low tip
Current method	0.1064	0.1078	−0.1349	−0.1264
FE simulation	0.1044	0.1059	−0.1313	−0.1228

The shape of the crack, not just its size, appears to affect the crack propagation potential. For example, Example #2 has provided that the normalized SIF for mode I fracture for the railhead containing a VSH defect is 0.086. The curved crack in Example #3 has shown that the normalized SIF for mode I fracture is 0.106 that is some 19% higher than that of the VSH defect, although both the VSH and curved cracks are 3 mm long each.

4. Conclusions

A new analytical method to solve singular integral equations is developed which extends the distributed dislocation method to examine curved cracks in finite geometries of arbitrary shapes. It is proved in this paper that this method can produce very accurate solutions for stress fields and crack tip parameters. The method of distributed dislocations is elegant, easy to use and does not require meshing that consumes significant human time.

A crack problem for railhead was studied. It is found that the normalized SIF for mode I fracture for railhead containing a VSH defect is the maximum. As the angle of inclination increases, it has been found that the normalized SIF for mode I fracture decreases in such a way that when the angle is larger than 24°, the crack would close. The SIF for mode II fracture, however, has been found to increase with the increase in the angle of inclination of the crack. When the crack is curved in such a way that its tips point vertically (up or down), the normalized SIF for mode I fracture has been found to be some 19% larger than that corresponding to the VSH defect.

Acknowledgement

The RAAS Grants Scheme of the Central Queensland University funded this project.

References

Bilby, B.A., Eshelby, J.D., 1968. Dislocations and the theory of fracture. In: Liebowitz, H. (Ed.), Fracture, vol. I. Academic Press, New York. pp. 99–182.

Bilby, B.A., Cottrell, A.H., Swinden, K.H., 1963. The spread of plastic yield from a notch. Proceedings of the Royal Society of London Series A 272, 304–314.

Comninou, M., Chang, R.-K., 1985. Effects of partial closure and friction on a radial crack emanating from a circular hole. International Journal of Fracture 28, 29–36.

Comninou, M., Schmeuser, D., 1979. The interface crack in a combined tension–compression and shear field. Journal of Applied Mechanics 46, 345–348.

Dai, D.N., 2002. Modelling cracks in finite bodies by distributed dislocation dipoles. Fatigue and Fracture of Engineering Materials and Structures 25, 27–39.

Erdogan, R., Gupta, G.D., 1971. Layered composites with an interface flaw. International Journal of Solids and Structures 7, 1089–1107.

Erdogan, F., Gupta, G.D., Ratwani, M., 1974. Interaction between a circular inclusion and an arbitrarily oriented crack. Journal of Applied Mechanics 41, 1007–1013.

Freund, L.B., Kim, K.S., 1991. Spiral cracking around a strained cylindrical inclusion in a brittle material and its implications for vias in integrated circuits. Materials Research Society Proceedings 226, 291–302.

Han, J.J., Chen, Y.H., 2000. Interface crack interacting with a microvoid in the near-tip process zone. International Journal of Fracture 102, 223–244.

Hills, D.A., Comninou, M., 1985. A normally loaded half-plane with an edge crack. International Journal of Solids and Structures 21, 399–410.

Moes, N., Dolbow, J., Belytschko, T., 1999. A finite element method for crack growth without remeshing. International Journal for Numerical Methods in Engineering 46, 131–150.

Murakami, Y., Nasebe, N., et al., 1987. In: Stress Intensity Factors Handbook, vol. 2. Pergamon Press, Oxford, New York, Seoul, Tokyo.

Murakami, Y., Nasebe, N., et al., 1992. In: Stress Intensity Factors Handbook, vol. 3. Pergamon Press, Oxford, New York, Seoul, Tokyo.

Muskhelishvili, N.I., 1963. Some Basic Problems of Mathematical Theory of Elasticity, fourth ed. Noordhoff, The Netherlands.

Nowell, D., Hills, D.A., 1987. Open cracks at or near free edges. Journal of Strain Analysis 22, 177–185.

Profillids, V.A., 1995. Railway Engineering. Avebury Technical, Aldershot, Brookfield USA, Hong Kong, Singapore, Sydney.

Sheng, C.F., 1987. Boundary element method by dislocation distribution. ASME Journal of Applied Mechanics 54, 105–109.

Shih, C.F., Asaro, R.J., 1988. Elastic-plastic analysis of cracks on bimaterial interfaces. Part I. Small scale yielding. Journal of Applied Mechanics 55, 299–316.

Sih, G.C., 1962. On the singular character of thermal stresses near a crack tip. ASME Journal of Applied Mechanics 29, 587–589.

Xiao, Q.Z., Dhanasekar, M., 2002. Coupling of FE and EFG using collocation approach. Advanced in Engineering Software 33, 507–515.

Zhao, L.G., Chen, Y.H., 1997. On the contribution of sub interface microcracks near the tip of an macrocrack to the J-integral in the bimaterial solids. International Journal of Engineering Science 35, 387–407.